Time-dependent analysis of the Coulomb breakup method for determining the astrophysical *S* factor

V. S. Melezhik[1,2] and D. Baye[1]
[1]*Physique Nucléaire Théorique et Physique Mathématique, C.P. 229, Université Libre de Bruxelles, B 1050 Brussels, Belgium*
[2]*Joint Institute for Nuclear Research, Dubna, Moscow Region RU-141980, Russian Federation*
(Received 05 June 2001; published 19 October 2001)

The time-dependent mesh method is applied to the calculation of the Coulomb breakup of a projectile into two charged fragments. The projectile is described in the potential model and its center of mass is assumed to follow a classical trajectory. The approach is compared with the first-order time-dependent perturbation approximation based on an electric dipole interaction under the same model assumptions. The numerical technique is applied to the $^{17}\mathrm{F}+{}^{208}\mathrm{Pb}\rightarrow{}^{16}\mathrm{O}+p+{}^{208}\mathrm{Pb}$ breakup in order to test the validity of the extraction of the $E1$ astrophysical S factor for the $^{16}\mathrm{O}(p,\gamma)^{17}\mathrm{F}$ radiative capture reaction to the $^{17}\mathrm{F}$ ground state. After carefully testing the validity of the numerical technique, we show that the accuracy of the astrophysical S factor extracted in such a way is better than 5% for projectile velocities above about $0.25c$ in large domains of impact parameters and relative energies between the fragments. Breakup cross sections are also calculated as a function of the relative energy between the fragments at different projectile velocities. A test calculation is performed for the breakup of the weakly bound $1/2^+$ excited state of $^{17}\mathrm{F}$. A comparison is presented and discussed with the only existing experimental differential cross section at the projectile energy of 10 MeV/nucleon.

DOI: 10.1103/PhysRevC.64.054612 PACS number(s): 25.60.Gc, 25.70.De, 25.40.Lw, 02.70.Jn

I. INTRODUCTION

Coulomb breakup has become an essential tool in several domains of nuclear physics. Breakup cross sections provide useful information about the structure of halo nuclei [1]. They can also be used as an indirect method of measurement of astrophysical S factors [2,3]. This topic is the subject of intensive experimental [4–11] and theoretical [12–19] investigations. Indeed the Coulomb field of the target nucleus simulates a large number of photons. The photodisintegration process is enhanced with respect to the time-reversed radiative capture by kinematic factors. However, the accuracy of the extracted astrophysical S factor cannot easily be established. Higher-order multipolarities, which are negligible in the capture process, may play a significant role in Coulomb breakup. The importance of the $E2$ component for the $^8\mathrm{B}$ breakup has been discussed by several authors but remains uncertain [12–16,19]. For this reason, this indirect method is not always considered as competitive with direct methods of measurement [20]. Testing the validity of this approach is usually based on an evaluation of the importance of higher-order corrections. A completely different approach will be followed in the present paper. We shall perform a calculation of Coulomb breakup, which is not based on a perturbative scheme nor on a multipole expansion. From this study, we shall deduce domains of projectile velocities, impact parameters and relative energies between the fragments where the accuracy of a determination of the astrophysical S factor from Coulomb breakup is better than some required value.

To this aim, we shall perform a numerical solution of the time-dependent Schrödinger equation describing the behavior of a two-body projectile in the varying Coulomb field induced by the target nucleus. To a good approximation, the breakup is a transition from a two-particle bound state to the continuum. The numerical method that we use has already been applied in Ref. [21] to the Coulomb breakup of $^{11}\mathrm{Be}$ into $^{10}\mathrm{Be}$ and one neutron in the Coulomb field of $^{208}\mathrm{Pb}$. In the present work, both fragments of the projectile are charged contrary to the halo nucleus breakup where a neutron is emitted. The fact that additional Coulomb interactions now appear between the projectile fragments on one hand, and between both fragments and the target on the other hand, does not lead to modifications of the computational scheme describing the time evolution of the wave packet. However, the analysis of this wave packet after the collision process requires taking accurately into account the nuclear and Coulomb distortion of the wave functions describing the relative motion between the projectile fragments. This will allow us to compare the obtained results with the first-order perturbation approximation, which is the basis of Coulomb breakup determinations of S factors.

The present test of the validity of the Coulomb breakup technique presents several advantages due to the fact that most model assumptions are identical in the compared numerical and perturbative approaches. More precisely, both calculations involve (i) the same nonrelativistic assumption, (ii) the same classical trajectory (a straight line in the following comparison), (iii) the same potential between the projectile components, and (iv) neglecting in the same way the nuclear interaction between the target and projectile. This implies that inaccuracies due to those simplifying model assumptions are of the same order in the compared numerical and perturbative approaches and will essentially cancel each other during the comparison of the nonperturbative and perturbative calculations. In other words, the perturbative approximation is the exact limit of our calculation and the domain of calculation conditions, where both approaches agree,

must have a physical significance. Moreover, the radiative capture cross section can be calculated within any necessary accuracy, under these model assumptions. If the potential model describing the system does not perfectly reproduce the experimental astrophysical S factor of the studied radiative capture reaction, the inaccuracies on the potential-model S factor should also not significantly affect the physical validity of the conclusions of the comparison.

Of course, the present model also has some limitations. The motion of the projectile is described by a classical trajectory. We have checked in Ref. [21] that straight-line and Coulomb trajectories give very close results at the velocities that we consider here. Except in Sec. V G, the following results are obtained with straight-line trajectories. However, the semiclassical approximation does not allow studying final-state three-body Coulomb effects. These effects have been analyzed by other authors [22].

In the present work, the time-dependent Schrödinger equation is solved on a three-dimensional spatial mesh. The potential only enters through its values at mesh points so that it can be easily modified. The fact that both fragments are charged can thus be introduced without complication. The method [23,24] makes use of values of the wave function at mesh points in angular space. The radial functions are approximated with variable-step finite-difference techniques. The accuracy of the treatment of the radial mesh is improved with respect to Ref. [21].

The Coulomb breakup reaction that we treat is $^{17}\mathrm{F}+{}^{208}\mathrm{Pb}\rightarrow{}^{16}\mathrm{O}+p+{}^{208}\mathrm{Pb}$. It is an interesting example for several reasons. The $^{16}\mathrm{O}(p,\gamma)^{17}\mathrm{F}$ radiative capture has been thoroughly studied experimentally [25,26,20] and is well understood theoretically [27–29]. Notice that this capture reaction dominantly proceeds towards the weakly bound $1/2^+$ excited state of $^{17}\mathrm{F}$ while only the ground-state capture can be studied with Coulomb breakup. The $^{16}\mathrm{O}+p$ system contains a closed-shell core and should rather well be described by a simple cluster model. A potential is available that fits the spectra of the $^{16}\mathrm{O}+p$ and $^{16}\mathrm{O}+n$ systems [30]. Finally, beams of $^{17}\mathrm{F}$ are becoming available. An experiment has already been performed near 10 MeV per nucleon [7].

In Sec. II, the physical problem is recalled and modelized. In Sec. III, the electric dipole first-order perturbation approximation whose validity is tested is described. The computational algorithm is summarized in Sec. IV. The $^{17}\mathrm{F}+{}^{208}\mathrm{Pb}\rightarrow{}^{16}\mathrm{O}+p+{}^{208}\mathrm{Pb}$ Coulomb breakup reaction is studied in detail in Sec. V. After some tests of the accuracy of the numerical approach, the obtained results are discussed and, in one case, compared with experiment. Section VI is devoted to concluding remarks.

II. BREAKUP MODEL

The projectile (P) is a bound system made of the core (c) and fragment (f) nuclei, which are treated as structureless particles. They interact through the potential $V(\boldsymbol{r})$, where $\boldsymbol{r}$ is the coordinate between the core and the fragment. If the target motion is described by a classical trajectory in the projectile rest frame, the breakup reaction on the target (T) follows the time-dependent Schrödinger equation

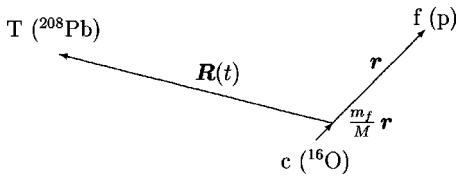

FIG. 1. Coordinates appearing in the definition of potential V_C [Eq. (3)].

$$i\hbar\frac{\partial}{\partial t}\Psi(\boldsymbol{r},t)=[H_0(\boldsymbol{r})+V^C(\boldsymbol{r},t)]\Psi(\boldsymbol{r},t), \tag{1}$$

where the wave packet $\Psi(\boldsymbol{r},t)$ describes the relative motion of the fragment and the core. In this expression,

$$H_0=-\frac{\hbar^2}{2\mu}\Delta_{\boldsymbol{r}}+V(\boldsymbol{r}) \tag{2}$$

is the projectile internal Hamiltonian with reduced mass $\mu=m_f m_c/M$, where m_f, m_c, and $M=m_f+m_c$ are the fragment, core, and projectile masses, respectively. The potential $V(\boldsymbol{r})$ is the sum of a central potential $V_0(r)$ including a Coulomb term tending towards $Z_f Z_c e^2/r$ when r is large and of a spin-orbit interaction $V_{\mathrm{so}}(r)$ coupling the relative orbital momentum $\boldsymbol{l}$ with the spin $\boldsymbol{I}_f$ of the fragment. Both form factors $V_0(r)$ and $V_{\mathrm{so}}(r)$ may depend on the orbital momentum quantum number l. The interaction $V^C(\boldsymbol{r},t)$ of the target nucleus with the projectile is assumed to be purely Coulombic. Notice that the introduction of nuclear interactions would be easy in the present model.

The time-dependent Coulomb potential $V^C(\boldsymbol{r},t)$ is defined as

$$V^C(\boldsymbol{r},t)=\frac{Z_c Z_T e^2}{|m_f\boldsymbol{r}/M+\boldsymbol{R}(t)|}+\frac{Z_f Z_T e^2}{|m_c\boldsymbol{r}/M-\boldsymbol{R}(t)|}-\frac{(Z_c+Z_f)Z_T e^2}{R(t)}, \tag{3}$$

where Z_f, Z_c, and Z_T are the charge numbers of the fragment, core, and target, respectively, and $\boldsymbol{R}(t)$ is the relative coordinate between the projectile and the target (see Fig. 1). The projectile center of mass is assumed to follow a classical trajectory with the initial velocity $\boldsymbol{v}$ at the impact vector $\boldsymbol{b}$.

The eigenfunctions of Hamiltonian H_0 with energy E are denoted as $\phi_{ljm}(E,\boldsymbol{r})$,

$$H_0\phi_{ljm}(E,\boldsymbol{r})=E\phi_{ljm}(E,\boldsymbol{r}), \tag{4}$$

where l is the relative orbital momentum, j is the total angular momentum resulting from the coupling of l with the spin I_f of the fragment, and m is its projection. The wave function $\phi_{ljm}(E,\boldsymbol{r})$ includes angular parts $Y_{lm_l}(\Omega)$ and fragment spin parts $|I_f m_f\rangle$ and reads in mixed notations

$$\phi_{ljm}(E,\boldsymbol{r})=r^{-1}u_{lj}(E,r)[Y_l(\Omega)\otimes|I_f\rangle]_{jm}. \tag{5}$$

Bound states are normed and scattering wave functions are normalized in such a way that

$$u_{lj}(E,r) \underset{r\to\infty}{\to} \cos\delta_l(E)F_l(E,r)+\sin\delta_l(E)G_l(E,r), \tag{6}$$

where F_l and G_l are the standard regular and irregular Coulomb functions [31] and δ_l is the phase shift.

The initial condition for solving Eq. (1) is then

$$\Psi^{(m_0)}(\boldsymbol{r},-\infty)=\phi_{l_0j_0m_0}(E_0,\boldsymbol{r}), \tag{7}$$

where E_0 and $l_0j_0m_0$ are the ground-state energy and quantum numbers, respectively. Equation (1) must be solved for each value of m_0. In practice, only positive values of m_0 need be considered, since results for negative values can be deduced from time reversal.

When the solution of Eq. (1) is known for $t\to\infty$, the breakup probability is obtained as a function of the impact parameter b as

$$\frac{dP}{dE}(E,b)=\frac{2\mu}{\pi\hbar^2k}\frac{1}{2j_0+1}\times\sum_{m_0}\sum_{ljm}|\langle\phi_{ljm}(E,\boldsymbol{r})|\Psi^{(m_0)}(\boldsymbol{r},+\infty)\rangle|^2 \tag{8}$$

with $E=\hbar^2k^2/2\mu$. In this expression, an average is performed over the possible values of m_0. The first factor is related to the choice of normalization (5) and (6) for the scattering waves of the core-fragment system. In Eq. (8), the final state is projected on the exact (distorted) scattering state of the core-fragment system at energy E. This is a generalization with respect to Refs. [21,32,33]. Such a generalization is essential to allow a comparison with the Coulomb breakup extraction of the astrophysical S factor. Notice another difference with earlier works: the wave function $\Psi^{(m_0)}(\boldsymbol{r},+\infty)$ need not be projected out of the bound-state subspace as, for example, $\Psi_{\rm bu}(\boldsymbol{r},+\infty)$ in Ref. [21]. Indeed the distorted final wave functions $\phi_{ljm}(E,\boldsymbol{r})$ for positive energies are automatically orthogonal to this subspace.

The breakup cross section can then be calculated as

$$\frac{d\sigma_{\rm bu}}{dE}(E)=2\pi\int_{b_{\min}}^{\infty}\frac{dP}{dE}(E,b)bdb. \tag{9}$$

The lower bound $b_{\min}$ is a cutoff related to the range of nuclear effects. The upper bound is in practice replaced by some value $b_{\max}$ whose choice must be carefully tested.

III. FIRST-ORDER PERTURBATION APPROXIMATION

The extraction of the $E1$ astrophysical S factor from breakup cross sections relies on the validity of the first-order perturbation approximation. Before describing the numerical algorithm for solving the time-dependent Schrödinger equation (1), let us summarize this simple approximation to which we shall compare our results in Sec. V.

At high enough velocities, Eq. (1) can be solved approximately by using the first-order perturbation theory [34,35] to give

$$\frac{dP^{(1)}}{dE}(E,b)=\frac{2\mu}{\pi\hbar^4k}\frac{1}{2j_0+1}\times\sum_{m_0}\sum_{ljm}\left|\int_{-\infty}^{\infty}\times e^{i\omega t}\langle\phi_{ljm}(E,\boldsymbol{r})|V^C|\phi_{l_0j_0m_0}(E_0,\boldsymbol{r})\rangle dt\right|^2, \tag{10}$$

where

$$\omega=(E-E_0)/\hbar. \tag{11}$$

When V^C is approximated by its external electric dipole term

$$V^C_{E1}=-Z_T\left(Z_c\frac{m_f}{M}-Z_f\frac{m_c}{M}\right)e^2\frac{\boldsymbol{r}\cdot\boldsymbol{R}(t)}{R(t)^3} \tag{12}$$

and the trajectory is a straight line

$$\boldsymbol{R}(t)=\boldsymbol{b}+\boldsymbol{v}t, \tag{13}$$

the time-dependent part of the integral in Eq. (10) contains the integrals

$$\int_{-\infty}^{\infty}e^{i\omega t}\frac{Y_{1q}[\Omega_R(t)]}{R(t)^2}dt=\sqrt{\frac{3}{4\pi}}\frac{2x}{bv}\left[K_0(x)\delta_{q0}-i\frac{q}{\sqrt{2}}K_1(x)\delta_{|q|1}\right], \tag{14}$$

where K_0 and K_1 are modified Bessel functions [31] and

$$x=\omega b/v. \tag{15}$$

Let us introduce the total $E1$ radiative capture cross section to the bound state $\phi_{l_0j_0m_0}(E_0,\boldsymbol{r})$,

$$\sigma_{E1}(E)=\frac{8\pi}{3kE}\left(Z_c\frac{m_f}{M}-Z_f\frac{m_c}{M}\right)^2e^2k_\gamma^3\times\frac{1}{(2I_c+1)(2I_f+1)}\times\sum_{m_0}\sum_{ljm}|\langle\phi_{l_0j_0m_0}(E_0,\boldsymbol{r})|\boldsymbol{r}|\phi_{ljm}(E,\boldsymbol{r})\rangle|^2. \tag{16}$$

The photon wave number is related to the initial energy E through $k_\gamma=(E+|E_0|)/\hbar c$. Combining Eqs. (10), (14), and (16) leads to the expression of the breakup probability [2,3]

$$\frac{dP^{(1)}_{E1}}{dE}(E,b)=\mathcal{N}(b)\frac{\mu}{\hbar^2}\frac{E}{E+|E_0|}\frac{(2I_c+1)(2I_f+1)}{2j_0+1}\sigma_{E1}(E). \tag{17}$$

In Eq. (17), the coefficient reads

$$\mathcal{N}(b)=\frac{Z_T^2\alpha}{\pi^2}\left(\frac{c}{v}\right)^4\{[K_0(x)]^2+[K_1(x)]^2\}, \tag{18}$$

where α is the fine structure constant. The $E1$ radiative cross section (16) can be calculated as [20,29]

$$\sigma_{E1}(E)=\frac{\alpha\hbar c}{2kE}N_{E1}k_\gamma^3[I_{E1}(E)]^2. \tag{19}$$

In Eq. (19), the normalization factor is given by

$$N_{E1}=\frac{16\pi}{3}\left(Z_c\frac{m_f}{M}-Z_f\frac{m_c}{M}\right)^2 \times\frac{(2j+1)(2j_0+1)(2l+1)(2l_0+1)}{(2I_c+1)(2I_f+1)} \times\begin{pmatrix} l_0 & 1 & l\\ 0 & 0 & 0\end{pmatrix}^2\begin{Bmatrix} j_0 & l_0 & I_f\\ l & j & 1\end{Bmatrix}^2. \tag{20}$$

The one-dimensional integral $I_{E1}(E)$ is given by

$$I_{E1}(E)=\int_0^\infty u_{l_0j_0}(E_0,r)ru_{lj}(E,r)dr, \tag{21}$$

where $u_{l_0j_0}(E_0,r)$ and $u_{lj}(E,r)$ are the radial parts of $\phi_{l_0j_0m_0}(E_0,\boldsymbol{r})$ and $\phi_{ljm}(E,\boldsymbol{r})$, respectively [Eq. (5)]. Notice that the normalization of the scattering wave function $u_{lj}(E,r)$ is the same as in Ref. [20] but differs from Ref. [29].

IV. NUMERICAL ALGORITHM

For solving the time-dependent four-dimensional Schrödinger equation (1), we apply a nonperturbative approach [24,21]. The angular part of the wave function is expanded over N angular basis functions $Y_\nu(\Omega)$, where N is a squared integer, $\Omega\equiv(\theta,\phi)$, and $\nu=(l,m_l)$. The angular basis consists in standard spherical harmonics $Y_{lm_l}(\Omega)$ with $|m_l|\leqslant\frac{1}{2}(\sqrt{N}-1)$ and $l\leqslant\sqrt{N}-1$, complemented by a few additional angular functions $\overline{Y}_{lm_l}(\Omega)$ with $\sqrt{N}\leqslant l\leqslant|m_l|+\sqrt{N}-1$ necessary to have the same number $\sqrt{N}$ of basis states for each of the $\sqrt{N}$ values of the projection m_l. The construction of the modified Legendre polynomial part of the $\overline{Y}_{lm_l}(\Omega)$ is explained in Ref. [21]. This angular basis is associated with a set of mesh points Ω_i in a two-dimensional angular grid. For the θ variable, the $\sqrt{N}$ mesh points are chosen as the zeros of the Legendre polynomial of degree $\sqrt{N}$. For the ϕ variable, the $\sqrt{N}$ mesh points are uniformly distributed over the unit circle. To this grid is associated a Gauss quadrature. The basis functions $Y_\nu(\Omega)$ are exactly orthonormal when their scalar product is calculated with this Gauss quadrature. The total number of grid points Ω_i is equal to the number N of basis functions in expansion (22) [23,24].

The wave function $\Psi(\boldsymbol{r},t)$ is expanded in spherical coordinates as

$$\Psi(\boldsymbol{r},t)=r^{-1}\sum_{m_f=-I_f}^{I_f}\sum_{\nu,i=1}^{N}Y_\nu(\Omega)(Y^{-1})_{\nu i}\psi_i^{m_f}(r,t)|I_fm_f\rangle. \tag{22}$$

In this section, the initial m_0 value on which $\Psi(\boldsymbol{r},t)$ and the $\psi_i^{m_f}(r,t)$ depend is understood. The coefficients $(Y^{-1})_{\nu i}$ are elements of the inverse of the matrix Y with elements $(Y)_{i\nu}=Y_\nu(\Omega_i)$. Notice that a misprint in the order of the subscripts of matrix φ in Ref. [21] is corrected here for Y. Each complex radial partial wave function $\psi_i^{m_f}(r,t)$ corresponds to the value of the component of $\Psi(\boldsymbol{r},t)$ with a specific projection m_f for the fragment spin I_f, calculated at the Ω_i mesh point,

$$\Psi(\boldsymbol{r},t)|_{\Omega=\Omega_i}=r^{-1}\sum_{m_f=-I_f}^{I_f}\psi_i^{m_f}(r,t)|I_fm_f\rangle. \tag{23}$$

The superscript m_f corresponds to the spin component while the subscript i refers to the angular mesh point.

Let us introduce the $(2I_f+1)N$-component vector $\boldsymbol{\Psi}(r,t)=\{\lambda_i^{1/2}\psi_i^{m_f}(r,t)\}$, where λ_i is the weight coefficient of the Gauss quadrature corresponding to the selected mesh [31] (see Ref. [21] for details). With respect to the unknown coefficients in expansion (22), the problem is reduced to a Schrödinger-type system of radial equations

$$i\hbar\frac{\partial}{\partial t}\boldsymbol{\Psi}(r,t)=[\hat{H}_0(r)+\hat{V}^C(r,t)]\boldsymbol{\Psi}(r,t). \tag{24}$$

In this system, $\hat{H}_0(r)$ and $\hat{V}^C(r,t)$ are $(2I_f+1)N\times(2I_f+1)N$ matrix operators representing H_0 [Eq. (2)] and V^C [Eq. (3)] on the grid. The elements of $\hat{H}_0(r)$ are defined by

$$H_{0ii'}^{m_fm_f'}(r)=-\frac{\hbar^2}{2\mu}\frac{\partial^2}{\partial r^2}\delta_{ii'}\delta_{m_fm_f'}+(\lambda_{i'}\lambda_i)^{-1/2} \times\sum_{\nu\nu'=1}^{N}(Y^{-1})_{\nu'i'}^{\star} \times\left\{\left[\frac{\hbar^2}{2\mu r^2}l(l+1)+V_0(r)\right]\delta_{\nu\nu'}\delta_{m_fm_f'}+V_{\rm so}(r) \times\langle lm_lI_fm_f|\boldsymbol{l}\cdot\boldsymbol{I}_f|lm_l'I_fm_f'\rangle\delta_{ll'}\right\}(Y^{-1})_{\nu i}, \tag{25}$$

where $V_0(r)$ and $V_{\rm so}(r)$ are the form factors for the potentials between the fragment and the core in the lth partial wave. Notice that the bracketed expression depends on ν and ν' through l, m_l and l', m_l'.

The elements of $\hat{V}^C(r,t)$ read

$$V_{ii'}^{Cm_fm_f'}(r,t)=V^C(r,\Omega_i,t)\delta_{ii'}\delta_{m_fm_f'}. \tag{26}$$

The Coulomb operator defined in Eq. (3) is diagonal in such a representation.

The time-dependent equations are solved as described in Sec. II C of Ref. [21]. The initial states are described at time $T_{\rm in}$ by the $(2j_0+1)/2$ ground-state wave functions $\phi_{l_0 j_0 m_0}(E_0,\boldsymbol{r})$ of H_0 with positive m_0 [Eq. (5)]. After a number of time steps Δt, each calculation is stopped at $T_{\rm out}$. It is shown in Ref. [24] that the computational time is approximately proportional to N when N is not too large.

For discretizing with respect to the radial variable r, a sixth-order (seven point) finite-difference approximation on a quasiuniform grid has been used on the interval $r\in[0,r_m]$. The grid has been realized by the mapping $r\rightarrow x$ of the initial interval onto $x\in[0,1]$ by the formula $r=r_m(e^{8x}-1)/(e^8-1)$ [23]. This is an important difference between Ref. [21] and earlier works [32,33] where uniform grids are used. The eigenvalue problem (4) for the initial bound state and for the final scattering states is solved on the same grid.

V. APPLICATION TO THE ^{17}F BREAKUP

A. Physical aspects

The present numerical technique is applied to the $^{17}\mathrm{F}+{}^{208}\mathrm{Pb}\rightarrow{}^{16}\mathrm{O}+p+{}^{208}\mathrm{Pb}$ breakup. The ^{17}F nucleus is well described by an $^{16}\mathrm{O}+p$ cluster structure. The ^{16}O core has spin 0 and the proton has spin $I_f=1/2$. The ^{17}F ground state with binding energy $|E_0|\approx 0.605$ MeV has quantum numbers $l_0=2$ and $j_0=5/2$. The energies of this $d5/2$ ground state and of the $s1/2$ bound excited state of ^{17}F are well reproduced by the potential of Ref. [30], which provides a simultaneous fit of the ^{17}O and ^{17}F single-particle levels. This potential contains central and spin-orbit terms, and a point-sphere Coulomb interaction. A Woods-Saxon form factor is used for the central part and its derivative for the spin-orbit part. All masses are integer multiples of the nucleon mass m_N fixed by $\hbar^2/2m_N=20.736$ MeV fm^2.

The $E1$ cross section for the $^{16}\mathrm{O}(p,\gamma)^{17}\mathrm{F}$ radiative capture reaction to the ^{17}F ground state contains two components with $l=1$ ($j=3/2$) and $l=3$ ($j=7/2$ and $5/2$). The $E1$ astrophysical S factor is related to this cross section by

$$S_{E1}(E)=Ee^{2\pi\eta}\sigma_{E1}(E), \tag{27}$$

where $\eta=Z_f Z_c e^2(\mu/2E\hbar^2)^{1/2}$. It can be calculated as explained in Ref. [20] for $E>0$ and in Ref. [29] for $E=0$. It is represented as a function of the relative energy E below 2 MeV in Fig. 2. The contributions of the p and f initial waves are displayed separately. The p wave capture dominates but the f component is not negligible at energies higher than 0.3 MeV. The theoretical curve underestimates the experimental data points of Ref. [26] by about 25% around 0.4–0.5 MeV and by progressively smaller amounts at higher energies. At low energies, this can be explained by an underestimation of the asymptotic normalization constant by the selected potential [27]. As emphasized in the Introduction, this should not affect comparisons between two different techniques of determination of the S factor. Finally, let us mention that higher multipole contributions to the S factor are negligible at the scale of the figure [28].

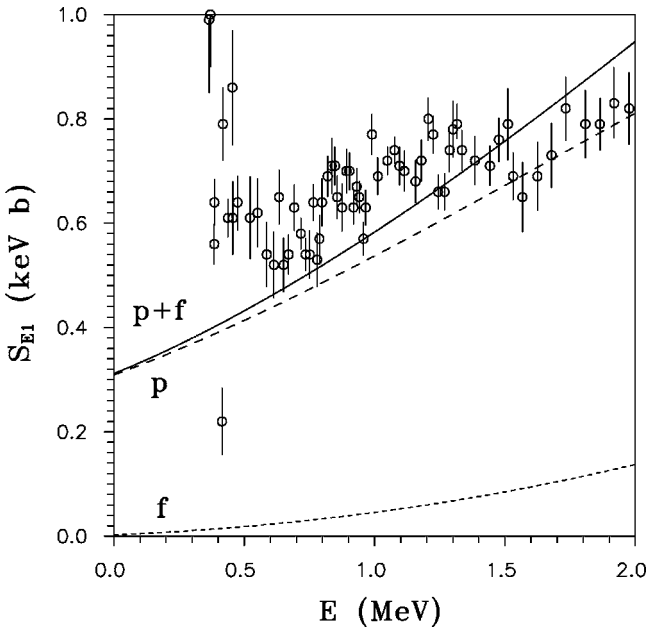

FIG. 2. $E1$ astrophysical S factor for the $^{16}\mathrm{O}(p,\gamma)^{17}\mathrm{F}$ radiative capture reaction to the ground state of ^{17}F (in keV b) as a function of the relative motion energy E (in MeV). The p wave (dashed line) and f wave (dotted line) contributions are also presented. The experimental data are from Ref. [26].

Let us introduce the quantity

$$S_{\rm bu}(E,b)=e^{2\pi\eta}\frac{2j_0+1}{(2I_c+1)(2I_f+1)}\frac{\hbar^2}{\mu}\frac{E+|E_0|}{\mathcal{N}(b)}\frac{dP}{dE}(E,b), \tag{28}$$

where the last factor is given by Eq. (8). This expression has the dimensions of an S factor. However, it depends on the selected impact parameter b. According to Eq. (17), when the first-order and $E1$ approximations are valid, i.e., when, respectively, the velocity v and the impact parameter b are large enough, the expression $S_{\rm bu}(E,b)$ should be nearly independent of b and equal to the $E1$ S factor (27).

B. Numerical aspects

The physical variables of the problem are the projectile velocity v, the relative energy E between the fragments, and the impact parameter b. The numerical method depends on a number of parameters: the initial time $T_{\rm in}$, the final time $T_{\rm out}$, the time step Δt, the number N of angular mesh points, the number N_r of radial discretization points, and the location r_m of the last radial mesh point. In this section, we briefly explain the choice of those values. Except otherwise indicated, trajectories are straight lines.

A first guess for the times $T_{\rm in}$ and $T_{\rm out}$ can be obtained by evaluating numerically the integrals

$$\int_{T_{\rm in}}^{T_{\rm out}} e^{i\omega t}\frac{Y_{1q}[\Omega_R(t)]}{R(t)^2}dt\approx\Delta t\sum_{j=1}^{N_t} e^{i\omega t_j}\frac{Y_{1q}[\Omega_R(t_j)]}{R(t_j)^2} \tag{29}$$

with $t_j = T_{\rm in} + (j-1/2)\Delta t$ and $N_t = (T_{\rm out} - T_{\rm in})/\Delta t$. The obtained values depend on v and must be valid for all selected b. With these starting values, full numerical tests have been performed by varying the parameters $T_{\rm in}$, $T_{\rm out}$, and Δt around the initial guesses. The value of Δt is 0.05 $\hbar$/MeV throughout.

For the Coulomb breakup evaluation of S factors, the calculations are performed with $T_{\rm out} = -T_{\rm in} = 30$ $\hbar$/MeV for $v/c \geqslant 0.25$ and 40 $\hbar$/MeV for $v/c < 0.25$. The number N of angular mesh points is 81, i.e., nine θ values and nine ϕ values. The corresponding basis includes all spherical harmonics with orbital momenta up to $l=4$ and some components up to $l=12$. The choice of a radial mesh is similar to the one in Ref. [21]: $r_m = 800$ fm and $N_r = 2000$.

For the calculation of cross sections, a good accuracy is obtained with $T_{\rm out} = -T_{\rm in} = 20$ $\hbar$/MeV, like in Ref. [21]. The number N of angular mesh points is 49, i.e., seven θ values and seven ϕ values. The corresponding basis includes all spherical harmonics with orbital momenta up to $l=3$ and some components up to $l=9$. The radial mesh is obtained with $r_m = 800$ fm and $N_r = 500$. The integrations over impact parameters are performed with $b_{\rm min} = 12$ fm and up to 110 fm with steps of 1 fm below 52 fm and 2 fm above that value.

C. Test with an electric dipole interaction

In Sec. III, two different approximations are described: first-order perturbation theory and electric dipole approximation. In order to disentangle their effects, we first perform numerical calculations with an $E1$ Coulomb potential. In other words, we numerically solve the Schrödinger equation

$$i\hbar \frac{\partial}{\partial t}\Psi(\boldsymbol{r},t) = [H_0(\boldsymbol{r}) + V^C_{E1}(\boldsymbol{r},t)]\Psi(\boldsymbol{r},t), \qquad (30)$$

which differs from Eq. (1) by the use of the approximate Coulomb potential (12). The resulting wave function can be used to measure the validity of first-order perturbations. Conversely, we can also use it to test the accuracy of the numerical scheme when the first-order approximation is accurate. The following conclusions will be improved in the next section when all multipoles will be taken into account.

The ratio $S_{\rm bu}/S_{E1}$ of the approximate S factor extracted from Coulomb breakup [Eq. (28)] calculated with the $E1$ potential V^C_{E1} [Eq. (12)] and of the exact $E1$ S factor within the present model [Eq. (19)] is presented in Fig. 3. For the highest colliding velocity $v/c = 0.3$, the Coulomb breakup S factor agrees with S_{E1} within 1% for the highest impact parameters ($b > 80$ fm) in the energy range $E = 0.3$–1.7 MeV. The value 1% can be considered as an upper bound of the accuracy of our calculation for that high velocity. At relative energies smaller than 0.3 MeV, the capture cross section becomes very small because of the effect of the Coulomb barrier. A reliable value for $S_{\rm bu}$ cannot be extracted from the small breakup component in the wave packet at those small energies. The small oscillation observed near 0.5 MeV for large b values originates from the same problem. For $E > 1.7$ MeV, the accuracy is also progressively reduced because the final relative scattering waves start oscillating more rapidly. The 1% numerical accuracy is obtained under the plausible assumption that the full line ($b = 100$ fm) should almost coincide with unity. Keeping in mind the 1% accuracy and using the full line as a reference, one obtains that $E1$ Coulomb breakup requires impact parameters larger than 50 fm to reach an accuracy of about 1% on the S factor at $v/c = 0.3$. A 5% accuracy is reached for all considered energies and impact parameters.

For $v/c = 0.25$, the breakup component is somewhat larger in the wave packet and the accuracy of the numerical technique is slightly better. The range of impact parameters for which the first-order approximation is valid within 1% is reduced to $b > 70$ fm. Here also a 5% accuracy is reached for all considered energies for $b \geqslant 40$ fm. For $v/c = 0.2$, the time evolution requires a larger $T_{\rm out}$. The validity of the first-order approximation is reduced both in energy and impact parameter. Only a small energy region ($0.5 < E < 1.0$ MeV) might provide the S factor to 1% for large impact parameters ($b \geqslant 70$ fm). Within 5%, impact parameters larger than 50 fm are enough on most of the energy range but the extraction of the S factor would involve some distorted energy dependence. At the lowest velocity that we have considered ($v/c = 0.15$), the accuracy of the S factor would become much poorer and the distortion more important. We can already say that this velocity is too low for astrophysical purposes.

Notice that a reasonable convergence with respect to $b \to \infty$ is obtained in all cases. This means that reliable cross sections can be obtained when performing numerically the integral in Eq. (9). The convergence becomes, however, slower when the projectile velocity decreases.

D. Validity of the Coulomb breakup approach

The results of the previous section were obtained with the $E1$ multipole only and are therefore not realistic. However they allow us to trust the results of calculations with the full Coulomb interaction.

The ratio $S_{\rm bu}/S_{E1}$ calculated with the full Coulomb potential V^C [Eq. (3)] is presented in Fig. 4. This ratio is useful to test the S factor determination from breakup differential cross sections. This technique is simulated here by the extraction of S_{E1} from dP/dE with Eq. (28). For the highest colliding velocity $v/c = 0.3$, the Coulomb breakup S factor becomes progressively smaller than S_{E1} when E increases. The contribution of higher multipoles (mostly $E2$ here) leads to an underestimation of the S factor. It reaches 1–3 % at most for impact parameters larger than 50 fm. A 5% accuracy is obtained over the full energy range for $b \geqslant 40$ fm.

The situation is similar at $v/c = 0.25$ but the systematic energy distortion becomes more important. Impact parameters larger than 60 fm should be used to get a 5% accuracy. At $v/c = 0.2$, the shape of the curves becomes similar to that observed in Fig. 3, but downscaled by more than 5%. The energy distortion is much stronger than at $v/c = 0.25$. Only very large impact parameters would allow keeping a 5% accuracy at that velocity. At $v/c = 0.15$, the role of higher multipoles is considerable. However, we could not get really

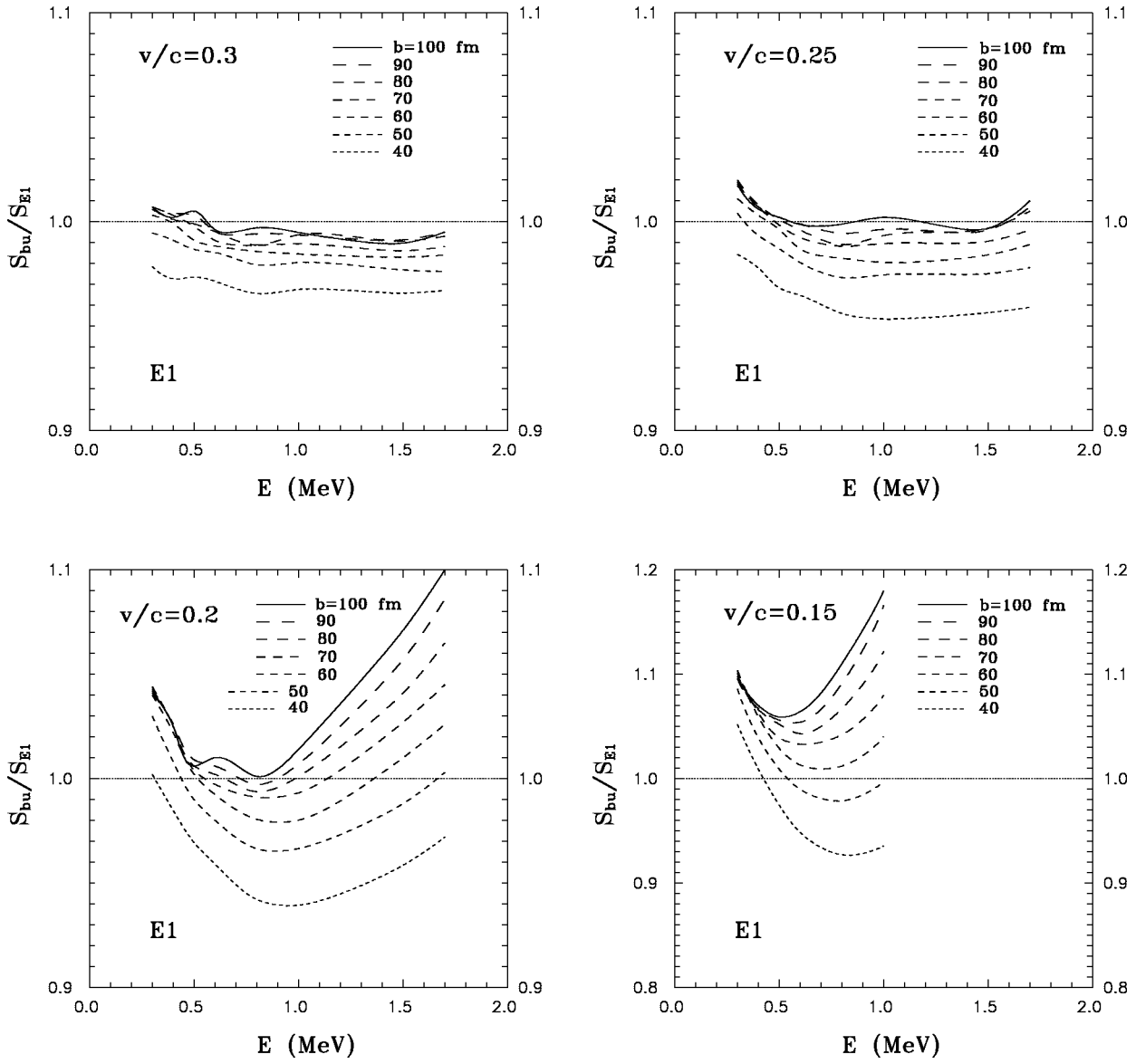

FIG. 3. Ratio S_{bu}/S_{E1} of the approximate S factor extracted from Coulomb breakup [Eq. (28)] calculated with the $E1$ potential V_{E1}^{C} [Eq. (12)] and of the exact $E1$ S factor within the present model [Eq. (19)]. The ratio is calculated for different projectile velocities v and impact parameters b. Notice the different vertical scale for $v/c=0.15$.

stable results for the largest b values, which are not shown. Anyway, as expected in the previous section, this velocity seems to be too low for a useful S factor extraction.

E. Breakup cross sections

Total breakup cross sections can be obtained by numerically integrating Eq. (9) over the impact parameter b. In Fig. 5, the convergence with respect to b is checked as a function of the relative energy E for a projectile energy of 72 MeV/nucleon. In the present nonrelativistic model, we consistently use $\epsilon=\frac{1}{2}m_N v^2$ for the laboratory projectile energy per nucleon. The value of 72 MeV/nucleon thus corresponds here to $v/c\approx 0.392$. The contribution of impact parameters larger than 50 fm is small and a good convergence is obtained for $b_{\max}=100$ fm.

The cross section at 72 MeV/nucleon peaks around $E=2.5$ MeV. We assume that it is somewhat underestimated at lower energies by an amount that can be obtained from the ratio of the theoretical and experimental S factors in Fig. 2. The breakup cross sections at different colliding energies are compared in Fig. 6. The cross section is slightly larger at 36 MeV/nucleon and somewhat smaller at 18 MeV/nucleon. The shape does not vary much, with a slow shift of the maximum towards larger E values when ϵ increases.

The ^{17}F nucleus possesses a single excited state near 0.5 MeV of excitation energy. The binding energy of this state is only 0.106 MeV. For this reason, this state has a broad spatial extension. We use the breakup of ^{17}F* as a preliminary convergence test for a calculation of the ^{8}B Coulomb breakup. This reaction is of prime significance to determine the S factor of the important $^{7}\mathrm{Be}(p,\gamma)^{8}\mathrm{B}$ radiative capture reaction.

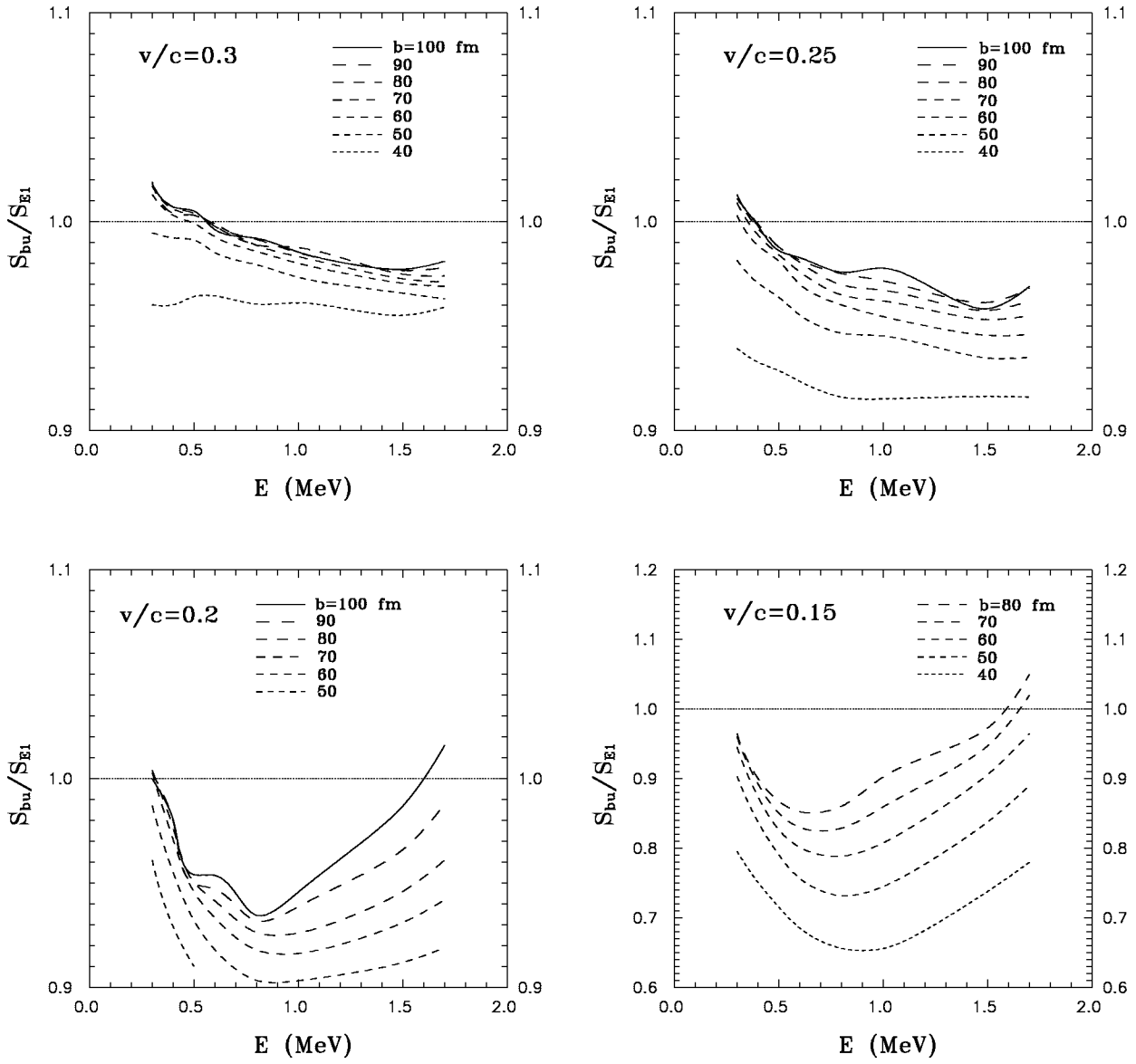

FIG. 4. Ratio S_{bu}/S_{E1} of the approximate S factor extracted from Coulomb breakup [Eq. (28)] calculated with the full Coulomb potential V^C [Eq. (3)] and of the exact $E1$ S factor within the present model [Eq. (19)]. The ratio is calculated for different projectile velocities v and impact parameters b. Notice the very different vertical scale for $v/c=0.15$.

It has been the object of many experimental [5,6,8,10] and theoretical [12–19] efforts. Some previous time-dependent calculations [13,15] were based on a multipole expansion of the Coulomb interaction. The present approach is not based on such an expansion, in addition to being nonpertubative. As a test of the validity of our method for the ^{8}B breakup, we have applied it to the breakup of ^{17}F* since the binding energies of this state and of ^{8}B are comparable. We have tested the accuracy of the ^{17}F* breakup cross section at high projectile velocity. We have found a much slower convergence of the integral (9) with respect to the impact parameter b. For keeping the same order of accuracy, we had to increase b_{max} to 200 fm, which renders the computation more time consuming. Nevertheless the breakup of a weakly bound state can be studied with the same accuracy as for the ^{17}F ground state and an accurate time-dependent study of the ^{8}B breakup is thus feasible with the full Coulomb interaction.

The ^{17}F* breakup cross section at 72 MeV/nucleon (scaled by 0.1) is represented as a dotted line in Fig. 6. As expected, it is much larger than for the ground state, by a factor of about 25. Although it is not experimentally measurable, it offers a testing ground for the accuracy of other methods based on perturbative and/or multipole expansions.

F. Inelastic cross section

The inelastic cross section to the $1/2^+$ excited state of ^{17}F is displayed in Fig. 7 as a function of the projectile energy per nucleon ϵ. This cross section is calculated as

$$\sigma_{1/2^+}(\epsilon)=2\pi\int_{b_{\mathrm{min}}}^{\infty}P_{s1/2}(b)bdb, \tag{31}$$

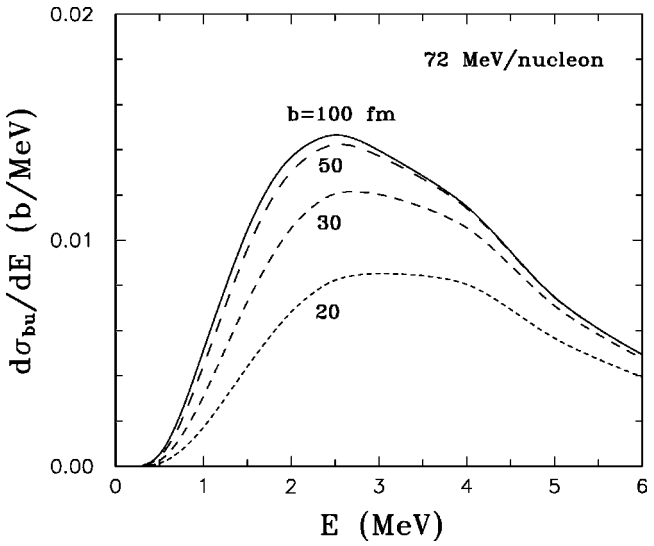

FIG. 5. Convergence with respect to the impact parameter b of the breakup cross section (in b/MeV) as a function of the relative energy E of the ^{16}O and proton fragments (in MeV) for a projectile energy of 72 MeV/nucleon ($v/c \approx 0.392$).

where the excitation probability of an lj bound state is given by

$$P_{lj}(b) = \frac{1}{2j_0+1} \sum_{m_0} \sum_{m} |\langle \phi_{ljm}(E,\boldsymbol{r}) | \Psi^{(m_0)}(\boldsymbol{r},+\infty)\rangle|^2. \tag{32}$$

Since the ground and excited states have angular momenta differing by two units and the same parity, the simplest transition mechanisms require an $E2$ transition or two successive

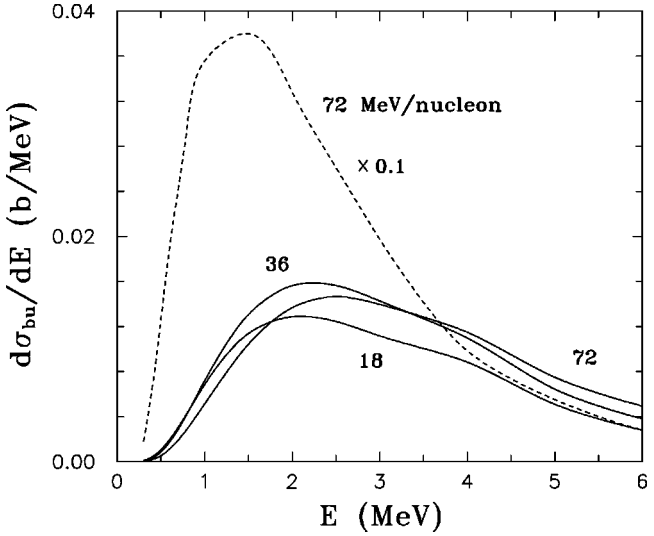

FIG. 6. Breakup cross section of ^{17}F (in b/MeV) as a function of the relative energy E (in MeV) for various projectile energies ϵ:18, 36, and 72 MeV/nucleon ($v/c \approx 0.196$, 0.277, and 0.392, respectively). The breakup cross section of ^{17}F* ($E_x = 0.495$ MeV) for the projectile energy 72 MeV/nucleon, scaled by 0.1, is represented as a dotted line.

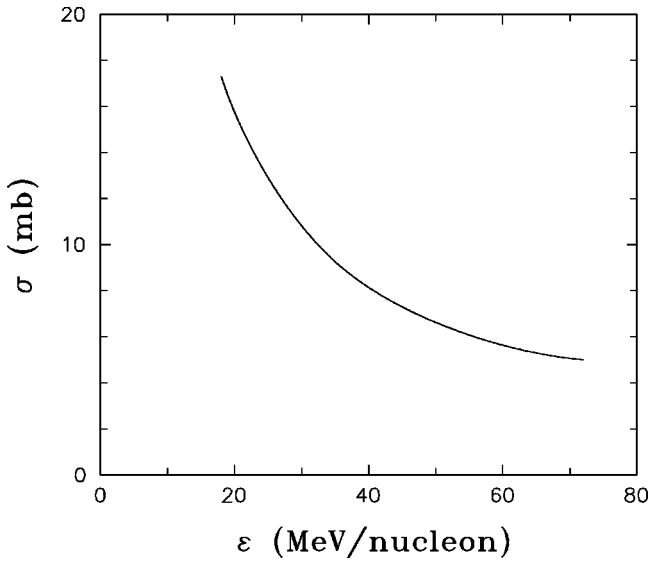

FIG. 7. Inelastic cross section to the $1/2^+$ excited state of ^{17}F (in mb) as a function of the projectile energy ϵ (in MeV/nucleon).

$E1$ transitions. The advantage of the present approach is that all mechanisms and all multipoles are automatically included.

One observes a regular decrease of the inelastic cross section over the considered energy range.

G. Comparison with experiment

Finally we perform a comparison with the only existing experimental data point [7] for the projectile energy of 10 MeV/nucleon (see Fig. 8). In fact this point has been analyzed in two different ways, with (full circle) and without (open circle) postacceleration correction.

In this section, because of the large values of the scattering angle, we use Rutherford trajectories with parameter

$$a = \frac{Z_T(Z_c+Z_f)e^2}{\mu_{\mathrm{TP}} v^2}, \tag{33}$$

where μ_{TP} is the target-projectile reduced mass. The calculation of the differential cross section is performed with the semiclassical approximation [34,35]

$$\frac{d\sigma}{d\Omega} = P_{\mathrm{bu}}(\theta) \frac{d\sigma_R}{d\Omega}, \tag{34}$$

where $d\sigma_R/d\Omega$ is the Rutherford cross section. The breakup probability P_{bu}, which depends here on the deflection angle θ, reads

$$P_{\mathrm{bu}}(\theta) = \int_0^\infty \frac{dP}{dE}[E, b(\theta)]dE. \tag{35}$$

By using the closure relation on the projectile states, this probability can be rewritten as a function of bound-state probabilities calculated like in Eq. (32) but with Coulomb trajectories, as

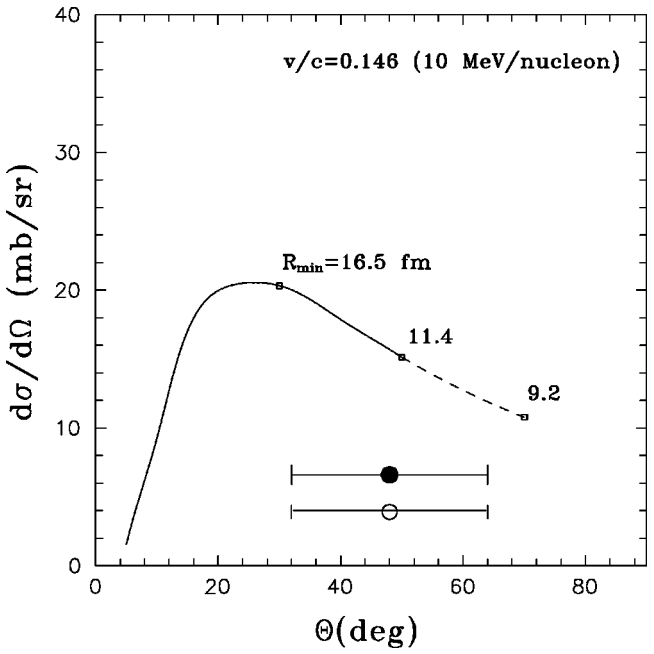

FIG. 8. Differential breakup cross section of ^{17}F (in mb/sr) as a function of the c.m. angle (in degrees) for the projectile energy 10 MeV/nucleon ($v/c \approx 0.146$). Different values of the distance $R_{\min}$ of closest approach are indicated. The experimental data points with (full circle) and without (open circle) postacceleration correction are from Ref. [7].

$$P_{\rm bu}(\theta) \approx 1 - P_{d5/2}[b(\theta)] - P_{s1/2}[b(\theta)]. \tag{36}$$

Equation (36) would be exact if the potential did not support additional bound states. Indeed the potential of Ref. [30] contains deep bound states in the $s1/2$, $p3/2$, and $p1/2$ partial waves, simulating Pauli forbidden states. These states are very weakly populated during the collision process. We have checked that Eqs. (35) and (36) are numerically equivalent in our model. Equation (36) is obviously easier to evaluate.

The differential breakup cross section of ^{17}F at 10 MeV/nucleon ($v/c \approx 0.146$) is displayed in Fig. 8 as a function of the c.m. deflection angle θ of the projectile. Notice that the fact that our approach includes all orders of perturbation and all multipoles is important at the experimental energy. Various mechanisms [7] such as direct and sequential breakup to single-particle states are automatically included. The calculated differential cross section displays a maximum near 20° like the results obtained in several models discussed in Ref. [7]. However the present calculated values are smaller and the disagreement with the experimental point is less important. In order to speculate on the origin of the discrepancy, several values of the distance of closest approach

$$R_{\min} = a(1 + \cot\tfrac{1}{2}\theta) \tag{37}$$

with $a \approx 3.1$ fm are shown in the figure. At the angular location of the experimental point, this distance is only about 11 fm so that the dotted part of the curve (at least) should be recalculated by including a nuclear interaction between the projectile and target. Therefore it is possible that the inclusion of nuclear effects might improve the agreement with experiment. This point requires further theoretical consideration but further experimental data would also be welcome.

VI. CONCLUSION

In this paper, we have improved and extended the numerical method presented in Ref. [21] to simulate the Coulomb breakup determination of an astrophysical S factor. To this end we have introduced a distortion of the scattering state between the fragments, which was not taken into account in Ref. [21]. The validity of the present approach has been tested with a purely $E1$ Coulomb interaction. It is remarkable that the S factor extracted by this technique from the theoretical breakup probabilities agrees within 1% with a direct and completely independent calculation of this S factor under the same model conditions.

The main simplifying assumption of the present model is probably the use of a classical trajectory in a time-dependent approach. Fixing this trajectory prevents studying the complicated three-body Coulomb effects in the final state. Nevertheless the present model takes into account the different (Coulomb and nuclear) postacceleration effects between the fragments of the projectile.

The main results of the present work concern the validity of the Coulomb breakup method for deriving the astrophysical S factor. The study is performed on the $^{17}\mathrm{F} + {}^{208}\mathrm{Pb} \rightarrow {}^{16}\mathrm{O} + p + {}^{208}\mathrm{Pb}$ reaction. The ^{17}F nucleus is a good example of weakly bound nucleus. It possesses a well-defined cluster structure. Moreover, beams of this unstable nucleus are now available. This reaction can, in principle, be used to determine the $^{16}\mathrm{O}(p,\gamma)^{17}\mathrm{F}$ radiative capture S factor to the ^{17}F ground state. We observe that a minimal velocity of $0.25c$ (about 30 MeV per nucleon) is necessary to get accurate information (better than 5%) on the extracted S factor. The impact parameter must be larger than 60 fm. It is interesting to note that, even with a purely $E1$ interaction (Fig. 3), higher-order effects become smaller than 5% only for $b > 40$ fm at this velocity. We have rather arbitrarily considered a 5% accuracy as a goal for the extraction of the astrophysical S factor. Domains of validity for other accuracies can be studied in a similar way from Figs. 3 and 4.

The present work opens the way to an analysis without multipole expansion of the breakup of ^{8}B, which is made numerically more difficult by the smaller binding energy with respect to ^{17}F. The Coulomb breakup of ^{8}B is of prime importance to determine the S factor of the $^{7}\mathrm{Be}(p,\gamma)^{8}\mathrm{B}$ radiative capture reaction [5]. As a preliminary test, we have calculated the Coulomb breakup of ^{17}F in its excited $1/2^{+}$ state whose binding energy is even smaller. Because of the weakness of the binding, this state is spatially quite extended, which renders the calculation more time consuming.

We performed a comparison with the only experimental point existing to date for the ^{17}F breakup on ^{208}Pb. Like other model approaches, we obtain too large a theoretical result but the disagreement with experiment is somewhat smaller than in other models. We speculate that the introduction of a nuclear interaction between projectile and target might still improve the situation.

ACKNOWLEDGMENTS

This text presents research results of the Belgian program P4/18 on interuniversity attraction poles initiated by the Belgian state Federal Services for Scientific, Technical and Cultural Affairs. V.S.M. acknowledges the support of the National Fund for Scientific Research (FNRS), Belgium and of the Belgian IAP program P4/18.

[1] I. Tanihata, J. Phys. G **22**, 157 (1996).
[2] G. Baur, C.A. Bertulani, and H. Rebel, Nucl. Phys. **A458**, 188 (1986).
[3] G. Baur and H. Rebel, Annu. Rev. Nucl. Part. Sci. **46**, 321 (1996).
[4] H. Utsunomiya, R.P. Schmitt, Y.-W. Lui, D.R. Haenni, H. Dejbakhsh, L. Cooke, P. Heimberg, A. Ray, T. Tamura, and T. Udagawa, Phys. Lett. B **211**, 24 (1988).
[5] T. Motobayashi, N. Iwasa, Y. Ando, M. Kurokawa, H. Murakami, J. Ruan (Gen), S. Shimoura, S. Shirato, N. Inabe, M. Ishihara, T. Kubo, Y. Watanabe, M. Gai, R.H. France III, K.I. Hahn, Z. Zhao, T. Nakamura, T. Teranishi, Y. Futami, K. Furutaka, and T. Delbar, Phys. Rev. Lett. **73**, 2680 (1994).
[6] N. Iwasa, F. Boué, G. Surówka, K. Sümmerer, T. Baumann, B. Blank, S. Czajkowski, A. Förster, M. Gai, H. Geissel, E. Grosse, M. Hellström, P. Koczon, B. Kohlmeyer, R. Kulessa, F. Laue, C. Marchand, T. Motobayashi, H. Oeschler, A. Ozawa, M.S. Pravikoff, E. Schwab, W. Schwab, P. Senger, J. Speer, C. Sturm, A. Surowiec, T. Teranishi, F. Uhlig, A. Wagner, W. Walus, and C.A. Bertulani, Phys. Rev. Lett. **83**, 2910 (1999).
[7] J.F. Liang, J.R. Beene, H. Esbensen, A. Galindo-Uribarri, J. Gomez del Campo, C.J. Gross, M.L. Halbert, P.E. Mueller, D. Shapira, D.W. Stracener, and R.L. Varner, Phys. Lett. B **491**, 23 (2000).
[8] J.J. Kolata, V. Guimarães, D. Peterson, P. Santi, R.H. White-Stevens, S.M. Vincent, F.D. Becchetti, M.Y. Lee, T.W. O'Donnell, D.A. Roberts, and J.A. Zimmerman, Phys. Rev. C **63**, 024616 (2001).
[9] Y. Tokimoto, H. Utsunomiya, T. Yamagata, M. Ohta, Y.-W. Lui, R.P. Schmitt, S. Typel, Y. Aoki, K. Ieki, and K. Katori, Phys. Rev. C **63**, 035801 (2001).
[10] B. Davids, D.W. Anthony, T. Aumann, S.M. Austin, T. Baumann, D. Bazin, R.R.C. Clement, C.N. Davids, H. Esbensen, P.A. Lofy, T. Nakamura, B.M. Sherrill, and J. Yurkon, Phys. Rev. Lett. **86**, 2750 (2001).
[11] T. Motobayashi, Nucl. Phys. **A693**, 258 (2001).
[12] K. Langanke and T.D. Shoppa, Phys. Rev. C **49**, R1771 (1994); **51**, 2844 (1995).
[13] C.A. Bertulani, Nucl. Phys. **A587**, 318 (1995).
[14] C.A. Bertulani, Z. Phys. A **356**, 293 (1996).
[15] H. Esbensen and G.F. Bertsch, Nucl. Phys. **A600**, 37 (1996).
[16] C.A. Bertulani and M. Gai, Nucl. Phys. **A636**, 227 (1998).
[17] H. Esbensen and G.F. Bertsch, Phys. Rev. C **59**, 3240 (1999).
[18] J.A. Tostevin, F.M. Nunes, and I.J. Thompson, Phys. Rev. C **63**, 024617 (2001).
[19] B. Davids, S.M. Austin, D. Bazin, H. Esbensen, B.M. Sherrill, I.J. Thompson, and J.A. Tostevin, Phys. Rev. C **63**, 065806 (2001).
[20] C. Angulo, M. Arnould, M. Rayet, P. Descouvemont, D. Baye, C. Leclercq-Willain, A. Coc, S. Barhoumi, P. Aguer, C. Rolfs, R. Kunz, J.W. Hammer, A. Mayer, T. Paradellis, S. Kossionides, C. Chronidou, K. Spyrou, S. Degl'Innocenti, G. Fiorentini, B. Ricci, S. Zavatarelli, C. Providencia, H. Wolters, J. Soares, C. Grama, J. Rahighi, A. Shotter, and M. Lamehi Rachti, Nucl. Phys. **A656**, 3 (1999).
[21] V.S. Melezhik and D. Baye, Phys. Rev. C **59**, 3232 (1999).
[22] E.O. Alt, B.F. Irgaziev, A.M. Mukhamedzhanov, and A.T. Muminov, in *the XVIIth European Conference on Few-Body Problems in Physics*, edited by A. Stadler *et al.* (Evora, Portugal, 2000), p. 248.
[23] V.S. Melezhik, Phys. Lett. A **230**, 203 (1997).
[24] V.S. Melezhik, in *Atoms and Molecules in Strong External Fields*, edited by P. Schmelcher and W. Schweizer (Plenum, New York, 1998), p. 89.
[25] C. Rolfs, Nucl. Phys. **A217**, 29 (1973).
[26] R. Morlock, R. Kunz, A. Mayer, M. Jaeger, A. Müller, J.W. Hammer, P. Mohr, H. Oberhummer, G. Staudt, and V. Kölle, Phys. Rev. Lett. **79**, 3837 (1997).
[27] D. Baye, P. Descouvemont, and M. Hesse, Phys. Rev. C **58**, 545 (1998).
[28] P. Descouvemont and D. Baye, Phys. Rev. C **60**, 015803 (1999).
[29] D. Baye and E. Brainis, Phys. Rev. C **61**, 025801 (2000).
[30] J.-M. Sparenberg, D. Baye, and B. Imanishi, Phys. Rev. C **61**, 054610 (2000).
[31] *Handbook of Mathematical Functions*, edited by M. Abramowitz and I.A. Stegun (Dover, New York, 1970).
[32] H. Esbensen, G.F. Bertsch, and C.A. Bertulani, Nucl. Phys. **A581**, 107 (1995).
[33] T. Kido, K. Yabana, and Y. Suzuki, Phys. Rev. C **50**, R1276 (1994); **53**, 2296 (1996).
[34] K. Alder, A. Bohr, T. Huus, B. Mottelson, and A. Winther, Rev. Mod. Phys. **28**, 432 (1956).
[35] K. Alder and A. Winther, *Electromagnetic Excitation* (North-Holland, Amsterdam, 1975).